The helimagnetic structure of $Eu(As_{0.20}P_{0.80})_3$ determined by zero-field neutron polarimetry

1997 J. Phys.: Condens. Matter 9 9167

(http://iopscience.iop.org/0953-8984/9/43/003)

J. Phys.: Condens. Matter **9** (1997) 9167–9173. Printed in the UK PII: S0953-8984(97)86180-2

The helimagnetic structure of $Eu(As_{0.20}P_{0.80})_3$ determined by zero-field neutron polarimetry

P J Brown†‡ and T Chattopadhyay†§

† Institut Laue–Langevin, BP 156, 38042 Grenoble Cédex 9, France
‡ Physics Department, Loughborough University, Leicester LE11 3TU, UK
§ Max-Planck-Institut für Physik Komplexer Systeme, Dresden, Germany

Received 21 July 1997

Abstract. Zero-field neutron polarimetric measurements have been made on semi-metallic phosphorus-rich $Eu(As_{1-x}P_x)_3$ with $x = 0.80$ to determine the magnetic structure of the low-temperature helimagnetic phase. Unlike unpolarized neutron diffraction, this technique allows an unambiguous determination of the spin configuration. We show that the previous structure model derived from unpolarized neutron diffraction data in which the Eu magnetic moments were assumed to be confined to the $\boldsymbol{a}$–$\boldsymbol{c}$ plane is not correct. The zero-field neutron polarimetric data clearly demonstrate the existence of a spin component parallel to the monoclinic $\boldsymbol{b}$-axis. The new model based on these observations is in better agreement with the diffraction intensities obtained from unpolarized neutron diffraction. In this model the low-temperature helimagnetic phase in phosphorus-rich $Eu(As_{1-x}P_x)_3$ has two components, one parallel to the $\boldsymbol{b}$-axis and a second which lies in the $\boldsymbol{a}$–$\boldsymbol{c}$ plane nearly perpendicular to the propagation vector.

1. Introduction

Ever since the pioneering experiment of Shull and Smart on MnO [1] the spin configuration of the magnetically ordered condensed state has traditionally been determined using unpolarized neutron diffraction intensities. Often the sample studied is polycrystalline and, although the technique works remarkably well for collinear spin structures, it often fails for a more complicated spin configuration, for example, non-collinear, incommensurate helimagnetic structure. For such structures even an unpolarized neutron diffraction investigation on good-quality single crystals may not yield a unique solution. For high-symmetry crystal structures the existence of several magnetic domains adds further uncertainty. Even traditional polarized neutron diffraction methods with one-dimensional polarization analysis on single crystals may fail to give a unique spin configuration.

In the present paper we demonstrate the power of zero-field three-dimensional neutron polarimetry in determining unambiguously the spin configuration of incommensurate modulated magnetic structures.

2. Previous work

Semi-metallic $EuAs_3$ forms a continuous series of solid solutions $Eu(As_{1-x}P_x)_3$ with an interesting magnetic phase diagram in which several modulated magnetic phases have been observed [2–5]. The solid solution retains the $EuAs_3$ structure [6] with space group $C2/m$ for x between 0 and 0.98. The magnetic properties of this system are unexpectedly

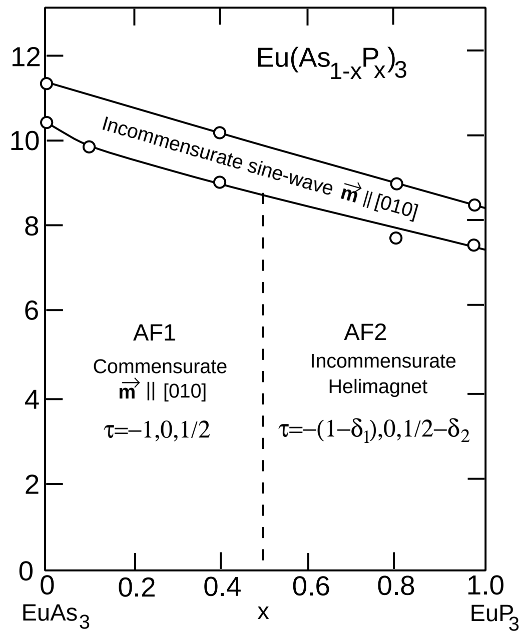

Figure 1. The magnetic (T, x) phase diagram of $Eu(As_{1-x}P_x)_3$, after [5].

complex for a Eu^{2+} ion in a spherically symmetric S state with no orbital moment. $EuAs_3$ orders at $T_N \approx 11$ K to a sine-wave amplitude-modulated structure in which the magnetic moments are parallel to the monoclinic $\boldsymbol{b}$-axis of the crystal. The periodicity of this modulated structure depends strongly on temperature and locks into a commensurate antiferromagnetic phase with propagation vector $\boldsymbol{\tau}_c = (-1, 0, \frac{1}{2})$ at $T_L = 10.3$ K. Arsenic-rich $Eu(As_{1-x}P_x)_3$ behaves similarly. Phosphorus-rich $Eu(As_{1-x}P_x)_3$ also orders at T_N to the sine-wave phase, but instead of locking into a commensurate phase undergoes a transition to a second incommensurate phase at a lower temperature. Figure 1 shows the (T, x) magnetic phase diagram of $Eu(As_{1-x}P_x)_3$. We have already studied the low-temperature magnetic structure of $Eu(As_{0.02}P_{0.98})_3$ using unpolarized neutron diffraction from a single crystal [5]. The propagation vector of the second incommensurate phase was found to be $\boldsymbol{\tau} = (-0.726, 0, 0.222)$ at 4.2 K. Intensities of 209 independent magnetic reflections were measured. Two structure models which retain the full monoclinic symmetry were tried. In the first (a) the spins are held in the $\boldsymbol{a}$–$\boldsymbol{c}$ plane and their directions are sinusoidally modulated (the helical or elliptic cycloidal model). In the second model (b), which is essentially the same as that for the higher-temperature phase, the spins are parallel to $\pm\boldsymbol{b}$ and their amplitude is modulated sinusoidally (the sine-wave model). In both models the pairs of Eu atoms related by the centre of symmetry at the origin have parallel spins, as in the antiferromagnetic commensurate phase of $EuAs_3$, but are modulated from cell to cell. Model (a) gave a significantly better agreement factor of $R = 0.15$ compared to the value $R = 0.21$ for model (b). We did not try any variation of model (a) in which the spins were not restricted to lying in the $\boldsymbol{a}$–$\boldsymbol{c}$ plane. Our resonant x-ray magnetic scattering investigations with polarization analysis [7] suggested that the magnetic structure of the helimagnetic phase of $Eu(As_{1-x}P_x)_3$ must contain a component of spin parallel to the $\boldsymbol{b}$-axis. However, this method could not give us any information about the actual magnetic structure. We have therefore undertaken a new study of the magnetic structure of the helimagnetic phase of Eu($As_{1-x}P_x$)$_3$ using zero-field neutron polarimetry [8] to carry out spherical polarization analysis of the magnetic elastic scattering.

3. Neutron polarimetry

3.1. Experimental details

The same small single crystal of Eu($As_{0.20}P_{0.80}$)$_3$ as was used in reference [5], of linear dimensions $1 \times 0.6 \times 4.5$ mm^3, was used for the present experiment. Its lattice parameters at 2 K are $a = 9.08$ Å, $b = 7.22$ Å, $c = 5.59$ Å, and $\beta = 112.95°$. Zero-field neutron polarimetry was carried out using Cryopad II [7] installed on the sample table of the polarized neutron triple-axis spectrometer IN20 at the Institut Laue–Langevin. The crystal was mounted with its b-axis vertical inside an ILL orange cryostat placed in the annular zero-field space of Cryopad II. For each of a number of $h0\ell$ reflections the direction of the scattered polarization was determined with the incident polarization successively parallel to the vertical direction ($\boldsymbol{z}$), the scattering vector ($\boldsymbol{x}$) and the third direction ($\boldsymbol{y}$) which completes the right-handed Cartesian set. These axes are the polarization axes and from their definition the magnetic interaction vector $\boldsymbol{Q}$ lies in the $\boldsymbol{y}$–$\boldsymbol{z}$ plane. The measurements were performed with a neutron wavelength of 1.53 Å. The polarization analysis showed that in all cases the directions of the incident and scattered polarization were parallel or antiparallel to within the experimental error. However, for incident polarization parallel to $\boldsymbol{y}$ or $\boldsymbol{z}$ the magnitude of the scattered polarization was significantly reduced and the degree of this depolarization varied for the different $h0\ell$ satellite reflections. The results are summarized in table 1 which gives the depolarization observed for the $\boldsymbol{y}$ and $\boldsymbol{z}$ incident directions for each reflection measured.

Table 1. Observed and calculated values of the depolarization with the incident beam polarized parallel to $\boldsymbol{x}$ and $\boldsymbol{z}$ for $h0\ell$ magnetic satellite reflections from Eu($As_{0.20}P_{0.80}$)$_3$.

			P_{obs}	P_{calc}	P_{obs}	P_{calc}
h	k	l	$\boldsymbol{y}$		$\boldsymbol{z}$	
−0.78	0.00	0.25	−0.1198	−0.0842	0.1150	0.0842
−3.22	0.00	−1.25	−0.1662	−0.1465	0.1725	0.1465
−1.22	0.00	0.75	−0.3832	−0.3783	0.3867	0.3783
−0.78	0.00	−0.75	−0.3331	−0.3621	0.3432	0.3621
−2.80	0.00	1.25	−0.1824	−0.1952	0.2254	0.1952
−3.20	0.00	1.75	−0.3343	−0.3028	0.3154	0.3028
−2.80	0.00	0.25	0.0282	0.0031	−0.0049	−0.0031
−3.20	0.00	−0.25	−0.0049	−0.0207	0.0248	0.0207

3.2. Analysis of the results

For a helical or cycloidal magnetic structure the magnetic moment on the ith sublattice of the jth unit cell of the structure may be written as

$$\boldsymbol{S}_{jl} = \boldsymbol{A}_j \cos(\boldsymbol{\tau} \cdot \boldsymbol{r}_l + \phi_j) + \mathrm{i}\boldsymbol{B}_i \sin(\boldsymbol{\tau} \cdot \boldsymbol{r}_j + \phi_j) \qquad (1)$$

where $\boldsymbol{A}_j$ and $\boldsymbol{B}_j$ are perpendicular vectors giving the magnitude and direction of the major and minor axes of the elliptical envelope of the spin modulation on the jth sublattice, $\boldsymbol{\tau}$ is the propagation vector of the modulation and $\boldsymbol{r}_l$ is the radius vector to the origin of the lth unit cell. The corresponding magnetic interaction vector is

$$\boldsymbol{Q}(\boldsymbol{k}) = \hat{\boldsymbol{k}} \times \left\{ \sum_{jl} f_i \exp\big[\mathrm{i}\boldsymbol{k}\cdot(\boldsymbol{r}_j + \boldsymbol{r}_l)\big]\big[\boldsymbol{A}_j \cos(\boldsymbol{\tau}\cdot\boldsymbol{r}_l + \phi_j) + \mathrm{i}\boldsymbol{B}_j \sin(\boldsymbol{\tau}\cdot\boldsymbol{r}_l + \phi_j)\big]\right\} \times \hat{\boldsymbol{k}}. \tag{2}$$

The f_j are the magnetic form factors, $\hat{\boldsymbol{k}}$ is a unit vector parallel to $\boldsymbol{k}$ and the sum is over all magnetic sublattices and all unit cells. The sums over the sublattices and the cells can be carried out in the usual way giving

$$\boldsymbol{Q}(\boldsymbol{k}) = \delta(\boldsymbol{g}, \boldsymbol{k} \pm \boldsymbol{\tau})(\boldsymbol{C} \pm \mathrm{i}\boldsymbol{D}) \tag{3}$$

where $\boldsymbol{g}$ is a reciprocal-lattice vector and

$$\boldsymbol{C} = \hat{\boldsymbol{k}} \times \sum_j f_j \boldsymbol{A}_j \exp(\mathrm{i}\boldsymbol{k}\cdot\boldsymbol{r}_j + \phi_j) \times \hat{\boldsymbol{k}} \tag{4}$$

$$\boldsymbol{D} = \hat{\boldsymbol{k}} \times \sum_j f_j \boldsymbol{B}_j \exp(\mathrm{i}\boldsymbol{k}\cdot\boldsymbol{r}_j + \phi_j) \times \hat{\boldsymbol{k}}. \tag{5}$$

For $Eu(As_{1-x}P_x)_3$ ($x \leqslant 0.98$) there are just two magnetic sublattices and they are related by the centre of symmetry at the origin. Assuming that the magnetic moments at these two sites have the same magnitude so that $\boldsymbol{A}_1 = \boldsymbol{A}_2 = \boldsymbol{A}$ and $\boldsymbol{B}_1 = \boldsymbol{B}_2 = \boldsymbol{B}$, the factors $\boldsymbol{C}$ and $\boldsymbol{D}$ have the form $\boldsymbol{C}'(a + \mathrm{i}b)$ and $\boldsymbol{D}'(a + \mathrm{i}b)$ where $\boldsymbol{C}'$ and $\boldsymbol{D}'$ are real vectors, $a = \cos(\psi_2 - \psi_1)$ and $b = \sin(\psi_2 - \psi_1)$ we have

$$\boldsymbol{Q}(\boldsymbol{g} + \boldsymbol{\tau}) = (\boldsymbol{C}' + \mathrm{i}\boldsymbol{D}')(a + \mathrm{i}b) \qquad \boldsymbol{Q}(\boldsymbol{g} - \boldsymbol{\tau}) = (\boldsymbol{C}' - \mathrm{i}\boldsymbol{D}')(a + \mathrm{i}b). \tag{6}$$

When, as in the present case, the magnetic scattering occurs at different $\boldsymbol{k}$ to that at which the nuclear scattering occurs, the expression for the cross-section for Bragg scattering of a neutron beam with polarization $\boldsymbol{P}_i$ is [9]

$$\frac{\partial\sigma}{\partial\Omega} = \boldsymbol{Q}\cdot\boldsymbol{Q}^* + \mathrm{i}\boldsymbol{P}_i\cdot(\boldsymbol{Q}^* \times \boldsymbol{Q}) \tag{7}$$

and the scattered polarization $\boldsymbol{P}_s$ is

$$\boldsymbol{P}_s \frac{\partial\sigma}{\partial\Omega} = \boldsymbol{Q}(\boldsymbol{P}_i\cdot\boldsymbol{Q}^*) + \boldsymbol{Q}^*(\boldsymbol{P}_i\cdot\boldsymbol{Q}) - \boldsymbol{P}_i(\boldsymbol{Q}\cdot\boldsymbol{Q}^*) - \mathrm{i}(\boldsymbol{Q}^* \times \boldsymbol{Q}). \tag{8}$$

The relationship between the polarizations of the incident and scattered beams may be described by the equation [10]

$$\boldsymbol{P}_{sj} = \mathsf{P}_{jk} P_{ik} + \boldsymbol{P}_{cj}.$$

The tensor P describes the effect of the scattering process on the magnitude and direction of an incident polarized, or partly polarized, beam and the vector $\boldsymbol{P}_c$ gives the polarization created in the scattering process. If the incident beam is nearly fully polarized, as in the present experiment, $\boldsymbol{P}_c$ can be neglected since no significant polarization can be created. For the sine-wave-modulated model, $\boldsymbol{A}$ is parallel to $\boldsymbol{b}$ ($\boldsymbol{z}$ for $h0\ell$ reflections) and $\boldsymbol{B}$ is zero. $\boldsymbol{C}'$ is parallel to $\boldsymbol{z}$ and $\boldsymbol{D}' = 0$. The cross-section is simply $\boldsymbol{Q}\cdot\boldsymbol{Q}^* = |\boldsymbol{C}'|^2(a^2 + b^2)$ and the polarization matrix has the elements

$$\begin{array}{lll} \mathsf{P}_{xx} = -1 & \mathsf{P}_{yx} = 0 & \mathsf{P}_{zx} = 0 \\ \mathsf{P}_{xy} = 0 & \mathsf{P}_{yy} = -1 & \mathsf{P}_{zy} = 0 \\ \mathsf{P}_{xz} = 0 & \mathsf{P}_{yz} = 0 & \mathsf{P}_{zz} = 1. \end{array} \tag{9}$$

The scattered beam is always fully polarized; it is parallel to the incident polarization for the $\boldsymbol{x}$- and $\boldsymbol{y}$-directions but reversed when the incident polarization is parallel to the spin direction $\boldsymbol{z}$. This is just the behaviour that we observed for the higher-temperature incommensurate phase of $Eu(As_{0.20}P_{0.80})_3$ and confirms that this does indeed have a sine-wave amplitude-modulated structure with spins parallel to $\boldsymbol{b}$.

For a spiral phase with no component of either $\boldsymbol{A}$ or $\boldsymbol{B}$ parallel to $\boldsymbol{b}$, $\boldsymbol{C}'$ and $\boldsymbol{D}'$ are parallel to one another and to the polarization axis $\boldsymbol{y}$ for all $h0\ell$ reflections; $\boldsymbol{Q}^* \times \boldsymbol{Q} = \mathbf{0}$, so the cross-section is simply $|\boldsymbol{Q}|^2$. The scattered polarization for the $h0\ell$ reflections is given by

$$\begin{array}{lll} \mathsf{P}_{xx} = -1 & \mathsf{P}_{yx} = 0 & \mathsf{P}_{zx} = 0 \\ \mathsf{P}_{xy} = 0 & \mathsf{P}_{yy} = 1 & \mathsf{P}_{zy} = 0 \\ \mathsf{P}_{xz} = 0 & \mathsf{P}_{yz} = 0 & \mathsf{P}_{zz} = -1. \end{array} \tag{10}$$

There is no depolarization even in the presence of chirality domains, and the incident and scattered polarizations are parallel for the $\boldsymbol{y}$-direction and antiparallel for the other two. This arrangement is therefore not compatible with our observations on the $h0\ell$ reflections of $Eu(As_{0.20}P_{0.80})_3$ in which a strong depolarization was observed in some reflections when the incident polarization was parallel to $\boldsymbol{y}$ or $\boldsymbol{z}$. It is clear therefore that one component of the modulated spins is parallel to $\boldsymbol{b}$. Assuming that this is $\boldsymbol{A}$, then for the $h0\ell$ reflections $\boldsymbol{C}'$ is parallel to $\boldsymbol{z}$ and $\boldsymbol{D}'$ to $\boldsymbol{y}$. The magnitude of $\boldsymbol{C}'$ is constant but that of $\boldsymbol{D}'$ varies from a maximum for reflections for which the scattering vector is nearly perpendicular to $\boldsymbol{B}$ to a minimum when it is nearly parallel. In this case the vector $\boldsymbol{Q}^* \times \boldsymbol{Q}$ is proportional to $|\boldsymbol{C}'||\boldsymbol{D}'|$ and its direction is parallel and antiparallel to $\boldsymbol{x}$ for the two chirality domains. Any inequality in the population of the chirality domains is given by the parameter α where

$$\alpha = \frac{V_+ - V_-}{V_+ + V_-} \tag{11}$$

and V_+ and V_- are the volumes of crystal belonging to the two domains. In this case the cross-section is $|\boldsymbol{C}'|^2 + |\boldsymbol{D}'|^2 \pm P_x|\boldsymbol{C}'||\boldsymbol{D}'|$ where the final term has opposite signs for the two domains. The scattered polarization is calculated from

$$\boldsymbol{P}_s = \frac{V_+(\boldsymbol{P}_s\, \partial\sigma/\partial\Omega)^+ + V_-(\boldsymbol{P}_s\, \partial\sigma/\partial\Omega)^-}{V_+(\partial\sigma/\partial\Omega)^+ + V_-(\partial\sigma/\partial\Omega)^-} \tag{12}$$

which, using equations (6), (7), (8) and (11), gives

$$\begin{array}{lll} \mathsf{P}_{xx} = -1 & \mathsf{P}_{yx} = 0 & \mathsf{P}_{zx} = 0 \\ \mathsf{P}_{xy} = \dfrac{2\alpha|\boldsymbol{C}'||\boldsymbol{D}'|}{|\boldsymbol{C}'|^2 + |\boldsymbol{D}'|^2} & \mathsf{P}_{yy} = -\dfrac{|\boldsymbol{C}'|^2 - |\boldsymbol{D}'|^2}{|\boldsymbol{C}'|^2 + |\boldsymbol{D}'|^2} & \mathsf{P}_{zy} = 0 \\ \mathsf{P}_{xz} = \dfrac{2\alpha|\boldsymbol{C}'||\boldsymbol{D}'|}{|\boldsymbol{C}'|^2 + |\boldsymbol{D}'|^2} & \mathsf{P}_{yz} = 0 & \mathsf{P}_{zz} = \dfrac{|\boldsymbol{C}'|^2 - |\boldsymbol{D}'|^2}{|\boldsymbol{C}'|^2 + |\boldsymbol{D}'|^2}. \end{array} \tag{13}$$

These equations explain the source of the depolarization in our measurements, since when $\alpha = 0$ the terms P_{xy} and P_{xz} which give rotation of the scattered polarization are zero, so the rotation of the polarization towards the scattering vector, characteristic of a helical modulation, is only observed through the depolarization of the scattered beam. The degree of depolarization is a measure of the difference $|\boldsymbol{C}'|^2 - |\boldsymbol{D}'|^2$.

The depolarization measurements for the set of $h0\ell$ reflections were used in a least-squares procedure to determine the ratio $\epsilon = \boldsymbol{A}/\boldsymbol{B}$ and the angle ψ which the vector $\boldsymbol{B}$ makes with the $\boldsymbol{c}$-axis. The final fit gave $\epsilon = 0.999(6)$, $\psi = -5.8(5)^\circ$ indicating that the envelope of the modulation is essentially circular with the normal to the plane in which the spins rotate lying in the $\boldsymbol{a}$–$\boldsymbol{c}$ plane at an angle of $18.1(6)^\circ$ to $\boldsymbol{a}$ in β obtuse. This is nearly

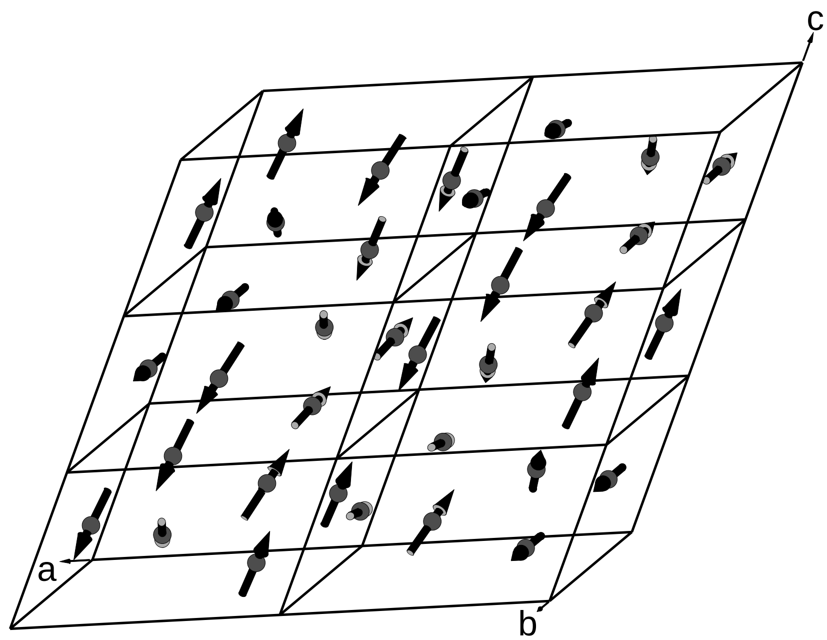

Figure 2. The schematic representation of the magnetic structure of the low-temperature helimagnetic phase of $Eu(As_{0.20}P_{0.80})_3$. Only the europium atoms are shown.

parallel to the propagation vector which is also in the $\boldsymbol{a}$–$\boldsymbol{c}$ plane and makes an angle of 9° with $\boldsymbol{a}$ in β acute. The values of the depolarization calculated for this model are given table 1.

4. The helimagnetic structure

Zero-field neutron polarimetry for the $Eu(As_{0.20}P_{0.80})_3$ single crystal clearly demonstrates that the low-temperature helimagnetic phase has a component of magnetic moment parallel to the monoclinic $\boldsymbol{b}$-axis. We have reanalysed the unpolarized neutron diffraction data of reference [5] for $Eu(As_{0.20}P_{0.80})_3$, introducing constraints to force compatibility with the conclusions drawn from the neutron polarimetry. The nuclear structure factors were used to determine the scale factor. The refinement with 46 symmetry-independent nuclear reflections gave an agreement factor of $R = 0.11$. Using the scale factor determined by this refinement and the 41 measured magnetic intensities, the low-temperature helimagnetic structure of $Eu(As_{0.20}P_{0.80})_3$ was also refined. The quality of the fit as indicated by the agreement factor $R = 0.12$ is comparable to that obtained for the nuclear structure. The magnetic moment per Eu atom was found to be $(7.4 \pm 0.3)\mu_B$ and the phase angle $\psi_2 - \psi_1$ was not significantly different from zero, indicating parallel coupling of the Eu sublattices related by the centre of symmetry at the origin. We conclude that the helimagnetic structure of $Eu(As_{0.20}P_{0.80})_3$, stable at low temperatures, can be described by two sinusoidal components of equal amplitude and frequency: one parallel to the monoclinic $\boldsymbol{b}$-axis and a second, in phase quadrature, lying in the $\boldsymbol{a}$–$\boldsymbol{c}$ plane nearly perpendicular to the propagation vector. Figure 2 shows a schematic representation of this structure.

Acknowledgments

We would like to thank F Tasset and T Roberts for their efforts in setting up Cryopad II and their support during the experiment.

References

[1] Shull C G and Smart J S 1949 *Phys. Rev.* **76** 1256
[2] Chattopadhyay T, Brown P J, Thalmeier P and von Schnering H G 1986 *Phys. Rev. Lett.* **57** 372
[3] Chattopadhyay T, Brown P J, Thalmeier P, Bauhofer W and von Schnering H G 1988 *Phys. Rev.* B **37** 269
[4] Chattopadhyay T and Brown P J 1988 *Phys. Rev.* B **38** 350
[5] Chattopadhyay T, Brown P J and von Schnering H G 1987 *Phys. Rev.* B **36** 7300
[6] Bauhofer W, Wittmann M and von Schnering H G 1984 *J. Phys. Chem. Solids* **42** 687
[7] Chattopadhyay T, Grübel G, Gibbs D, Rebelsky L and Axe J D 1990 unpublished results
[8] Brown P J, Forsyth J B and Tasset F 1993 *Proc. R. Soc.* A **442** 147
[9] Blume M 1963 *Phys. Rev.* **130** 1670
[10] Brown P J, Nunez V, Tasset F, Forsyth J B and Radhakrishna P 1990 *J. Phys.: Condens. Matter* **2** 9409